Advances in Aircraft and Spacecraft Science, *Vol. 10, No. 4 (2023) 347-368*
https://doi.org/10.12989/aas.2023.10.4.347

Static and modal analysis of bio-inspired laminated composite shells using numerical simulation

Faisal Baakeel[1], Mohamed A. Eltaher*[1], Muhammad Adnan Basha[1], Ammar Melibari[1] and Alaa A. Abdelrhman[2]

[1]*Mechanical Engineering Department, Faculty of Engineering, King Abdulaziz University, Jeddah, Saudi Arabia*
[2]*Mechanical Design and Production Department, Faculty of Engineering, Zagazig University, Zagazig, Egypt*

(Received April 3, 2023, Revised September 17, 2023, Accepted September 25, 2023)

Abstract. In the first part of this study, a numerical simulation model was developed using the mechanical APDL software to validate the results of the 3D-elastisity theory on the laminated sandwich plate developed by Panago. The numerical simulation model showed a good agreement to the results of Pagano's theory in terms of deflection, normal stresses, and shear stresses. In the second part of this study, the developed numerical simulation model was used to define different plates dimensions and fibers layup orientations to examine the load response in terms of deflection and stresses. Further analysis was implemented on the natural frequencies of laminated xxx plates of the plates. The layup configurations include Unidirectional (UD), Cross-Ply (CP), Quasi-Isotropic (QI), the linear bio-inspired known as Linear-Helicoidal (LH), and the nonlinear bio-inspired known as Fibonacci-Helicoidal (FH). The following numerical simulation model can be used for the design and study of novel, sophisticated bio-inspired composite structures in a variety of configurations subjected to sinusoidal or constant loads.

Keywords: bending and vibration; bio-inspired structures; composite materials; finite elements analysis; shell structure

1. Introduction

Composite materials are a combination of two or more materials that have different properties and characteristics. Composite materials offer considerable potential and design flexibility for high-performance structures. They are widely used in various industries, including marine structures, energy harvesters, automotive, spacecraft, aerospace, etc. (Melaibari *et al*. 2021). The demand for lightweight and high-performance structures in different industrial applications has provided a strong demand for the continuous development of composite materials. Composites consisting of a polymer matrix (e.g., epoxy) reinforced by fibers (e.g., glass, carbon) are among the common advanced composites that are classified as polymer matrix composites (PMCs). Carbon fiber reinforced polymer (CFRP) is most popular in advanced composites used in the industry due to its specific strength and excellent mechanical properties. The advantages of CFRP over conventional metals such as steel including; High Strength-to-Weight Ratio, Corrosion Resistance, Fatigue

*Corresponding author, Professor, E-mail: mohaeltaher@gmail.com, meltaher@kau.edu.sa

http://www.techno-press.org/?journal=aas&subpage=7 ISSN: 2287-528X (Print), 2287-5271 (Online)

Resistance, Design Flexibility (CFRP can be molded into complex shapes and designs), and Low Thermal-Conductivity (the thermal conductivity of CFRP ranges from 0.1 to 0.5 W/mK depending on the fiber orientation and resin matrix used, while the thermal conductivity of steel ranges from 15 to 50 W/mK depending on the alloy composition and temperature). Several arthropods, such as the Homarus americanus (American lobster), Callinectes sapidus (Atlantic blue crab), and Popillia japonica (the Japanese beetle), have hard exoskeletons that frequently exhibit exceptional structural qualities and multi-functional capabilities, including the ability to support the body weight, filter chemicals, and withstand external loads. Due to their potential to produce outstanding mechanical properties and adaptability for exoskeletons, the intrinsically complex hierarchical structures of various exoskeletons have recently attracted a lot of interest (Cheng *et al*. 2011).

Despite there being a lot of bio-inspired man-made structures studies, relatively little has been done to incorporate the design principles found in arthropod exoskeletons into the creation of useful materials and structures. It has been noticed that bio-inspired composite structures with helicoidal schemes have high-impact energy absorption. Thus, can result in better mechanical performance and load response. The study of shell theories enables one to comprehend plates, curved beams, and flat beams as special cases. Shells are curved structures with increased structural stiffness in comparison to plates in carrying loads and moments by a combined membrane and bending action because of their curvature (Mantari *et al*. 2011). Although the performance of the component can be obtained by analytical or experimental methods, it is more expensive and time-consuming. Therefore, numerical simulation can be a powerful tool in load response analysis and virtual design. Numerous review articles that describe the research on the analysis of laminated composite plates, beams, and shells under various loading circumstances related to this study can be found in the literature.

For the study of laminated structures, Reddy (1990) offered a comprehensive overview of shear deformation theories and their historical development. Carrera (2003) reviewed the theories that have been created for the analysis of multilayered structures, paying particular attention to the so-called "Zig-Zag" theories, which describe a piecewise continuous displacement field in the direction of plate thickness and fulfill interlaminar continuity of transverse stresses at each layer interface. Mantari *et al*. (2011) developed a new higher order shear deformation theory of sandwich composite plates and shells that accounts for an adequate distribution of the transverse shear strains through the plate thickness and the tangential stress-free boundary conditions on the plate boundary surface. Zhang and Yang (2009) published a literature review to the developed finite elements based on the various laminated plate theories for the free vibration and dynamics, buckling and post buckling analysis, geometric nonlinearity and large deformation analysis, and failure and damage analysis of composite laminated plates. Liew *et al*. (2011) reviewed various element-free or meshless methods and their applications in the analysis of laminated composite structures. Haldar and Bruck (2014) resulted that, due to the longitudinal reinforcement of pultruded carbon rod in foam core, a sandwich with a bio-inspired core offers better flexural strength and elastic energy absorption than a sandwich with a conventional un-reinforced core.

Bar-On *et al*. (2015) stated that different insect cuticles, osteons in mammalian bones, some plant cell walls, and DNA's structure are only a few examples of helical-shaped biologically laminated natural phenomena. It is well known that biological composite materials have properties such as creep, energy recovery, and vibration filtering. They are also strong, stiff, stable, and viscoelastic materials. Jayatilake *et al*. (2016) studied dynamic analysis of multilayer fibre composite sandwich plates with interlayer delaminations by using finite element method. Kaci *et al*. (2017) developed a finite element formulation to investigate the fracture toughness of composite aluminum plate under impact loads. Rachid *et al*. (2018) exploited classical version h and the version p of the finite element

method in analysis of dynamic response of tapered shaft rotor made of composite materials. Through numerical modeling, Abir *et al*. (2019) demonstrated how helicoidal architecture laminated plates improved impact resistance and energy absorption during the ballistic impact test. Bhaskar *et al*. (2019) developed the finite element model for geometrically nonlinear analysis of laminated plates using a new plate theory. Bahmani *et al*. (2019) developed 3D micromechanical assessment of bio-inspired composites with non-uniformly dispersed inclusions, which revealed the necessity to use 3D micromechanical models with realistic inclusion dispersions for accurately assessing the response of high inclusion volume fraction bio-inspired composites.

Han *et al*. (2020) investigated experimentally impact and bending properties of a novel dactyl-inspired sandwich honeycomb with carbon fiber. They found that the quasi-isotropic helicoidal arrangement of carbon fiber has an effective way to improve the impact resistance and bending energy absorption. Yang *et al*. (2020) provided a systematic analysis of the low-velocity impact response and energy absorption capacity of biomimetic architected CFRP laminates. Amorim *et al*. (2021) presented comprehensive review on bio-inspired approaches to enhance the toughening of fiber reinforced polymer composites and to give manufacturing solutions capable of mimicking biological material structures. Moosazadeh *et al*. (2021) studied the vibration and flutter og Two-dimensional curved panel in the frequency and time domain under thermal and in-plane load. Yang and Xie (2022) demonstrated the biomimetic Bouligand structure's strong thermal buckling behavior, opening the prospect of creating biomimetic composites with a favorable trade-off between mechanical and thermal performance. Lee *et al*. (2022) developed a high-throughput computer simulation that can be used to identify the best features incorporated in nacre-like structures and offer special design recommendations for the development of new impact-resistant materials.

Inspired by the non-linear helical structure of lobster, Han *et al*. (2022) designed and manufactured bioinspired fiber metal laminate with Janus helical structure through the method of hot press forming.

Magrini *et al*. (2022) examined the fracture behavior of hierarchical multi-layered bio-inspired composites comprising a polymer phase, which were inspired by the robust and durable hierarchical architecture of mollusk shells. By utilizing the Taguchi-Response surface approach, Sojobi and Liew (2022) were able to get excellent performance from bio-inspired prefabricated composites for durable and sustainable building. Mohamed *et al*. (2022a) studied numerically the bending, buckling and linear vibration of bio-inspired composite plates including Fibonacci sequence and got the optimum scheme of layer's orientation. Mohamed *et al*. (2022b) employed the bernstein polynomials in solving of the nonlinear bending and snap-through instability phenomena of curved bio-inspired composite beams with helicoidal orientation scheme. Almitani *et al*. (2022) provided the exact solutions for the nonlinear bending problem, the buckling loads, and postbuckling configurations of a perfect and an imperfect bio-inspired helicoidal composite beam with a linear rotation angle. Han *et al*. (2023), Zhang *et al*. (2023) designed and manufactured biomimetic laminated basalt fiber-reinforced composite through a method combining linear helicoidal layup and hot press forming. They investigated superior mechanical properties and microwave-transmissibility of these biomimetic laminated structures. Garg *et al*. (2023) investigated the buckling and free vibration response of bio-inspired laminated sandwich plates with helicoidal face sheets incorporating softcore using the finite element approach and higher-order zigzag theory.

According to previous works, the static and dynamic vibration behaviors of bioinspired composite plate using a finite element formulation have not been considered before. Therefore, the main objective of this study is to fill this gap. Accordingly, A FEA model will be constructed by

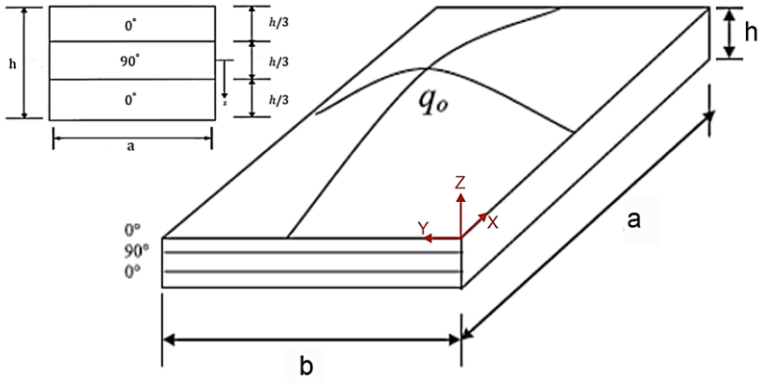

Fig. 1 Three-layered rectangular plate under static doubly sinusoidal load

utilizing the mechanical APDL software to numerically analyze the bending, natural frequencies, and vibration modes of bioinspired composite laminated plates. Different load profiles have been addressed. The rest of the article is organized as follows: the mathematical model and formulation including the kinematic equations, constitutive equations, and force/moment resultants are presented in section 2. Section 3 develops the finite element model used through the analysis. Validation with previous prestigious works has been illustrated in section 4 to confirm the obtained results. Numerical analysis and parametric studies have been presented in section 5.

2. Mathematical model and formulation

Fig. 1 shows the geometrical configuration of composite plates structures with length, width, and overall thickness (a, b, and h respectively). The displacement field of any point (x, y, z) can be found based on the first order shear deformation theory (FOSDT) by the following equations (Reddy *et al*. 2003)

$$\begin{Bmatrix} u(x,y,z,t) \\ v(x,y,z,t) \\ w(x,y,z,t) \end{Bmatrix} = \begin{Bmatrix} u_0(x,y,t) \\ v_0(x,y,t) \\ w_0(x,y,t) \end{Bmatrix} + z \begin{Bmatrix} \varphi_x(x,y,t) \\ \varphi_y(x,y,t) \\ 0 \end{Bmatrix} \tag{1}$$

In which u_0, v_0 represent the in-plane displacements and w_0 is the transverse displacement, φ_x and φ_y represent shear displacement at z=0. While the strain-displacement relations are portrayed by Mohamed *et al*. (2022b)

$$\begin{Bmatrix} \varepsilon_{xx} \\ \varepsilon_{yy} \\ \gamma_{xy} \\ \gamma_{xz} \\ \gamma_{yz} \end{Bmatrix} = \begin{Bmatrix} \frac{\partial u_0}{\partial x} + \frac{1}{2}\left(\frac{\partial w_0}{\partial x}\right)^2 + z\frac{\partial \varphi_x}{\partial x} \\ \frac{\partial v_0}{\partial y} + \frac{1}{2}\left(\frac{\partial w_0}{\partial y}\right)^2 + z\frac{\partial \varphi_y}{\partial y} \\ \frac{\partial u_0}{\partial y} + \frac{\partial v_0}{\partial x} + \frac{\partial w_0}{\partial x}\frac{\partial w_0}{\partial y} + z\left(\frac{\partial \varphi_x}{\partial x} + \frac{\partial \varphi_y}{\partial y}\right) \\ \varphi_x + \frac{\partial w_0}{\partial x} \\ \varphi_y + \frac{\partial w_0}{\partial y} \end{Bmatrix} \tag{2}$$

and the constitutive equations of composite plate are defined by Assie *et al*. (2011)

$$\begin{Bmatrix}\sigma_{xx}\\ \sigma_{yy}\\ \sigma_{xy}\end{Bmatrix}=\begin{bmatrix}\bar{Q}_{11} & \bar{Q}_{12} & \bar{Q}_{16}\\ \bar{Q}_{12} & \bar{Q}_{22} & \bar{Q}_{26}\\ \bar{Q}_{16} & \bar{Q}_{26} & \bar{Q}_{66}\end{bmatrix}\begin{Bmatrix}\varepsilon_{xx}\\ \varepsilon_{yy}\\ \gamma_{xy}\end{Bmatrix}$$
$$\begin{Bmatrix}\sigma_{yz}\\ \sigma_{xz}\end{Bmatrix}=\begin{bmatrix}\bar{Q}_{44} & \bar{Q}_{45}\\ \bar{Q}_{45} & \bar{Q}_{55}\end{bmatrix}\begin{Bmatrix}\gamma_{yz}\\ \gamma_{xz}\end{Bmatrix} \tag{3}$$

where the transformed material constants as a function of fiber orientation θ are evaluated as Karamanli *et al*. (2023)

$$\begin{aligned}\bar{Q}_{11} &= Q_{11}\cos^4(\theta)+(Q_{12}+2Q_{66})\sin^2(2\theta)+Q_{22}\sin^4(\theta)\\ \bar{Q}_{12} &= \tfrac{1}{2}(Q_{11}+Q_{22}-4Q_{66})\sin^2(2\theta)+Q_{12}\left(\sin^4(\theta)+\cos^4(\theta)\right)\\ \bar{Q}_{22} &= Q_{11}\sin^4(\theta)+(Q_{12}+2Q_{66})\sin^2(2\theta)+Q_{22}\cos^4(\theta)\\ \bar{Q}_{16} &= \tfrac{1}{2}\left[(Q_{11}-Q_{12}-2Q_{66})\cos^2(\theta)+(Q_{12}-Q_{22}+2Q_{66})\sin^2(\theta)\right]\sin(2\theta)\\ \bar{Q}_{26} &= \tfrac{1}{2}\left[(Q_{11}-Q_{12}-2Q_{66})\sin^2(\theta)+(Q_{12}-Q_{22}+2Q_{66})\cos^2(\theta)\right]\sin(2\theta)\\ \bar{Q}_{66} &= \tfrac{1}{2}(Q_{11}+Q_{22}-2Q_{12}-2Q_{66})\sin^2(2\theta)+Q_{66}\left(\sin^4(\theta)+\cos^4(\theta)\right)\\ \bar{Q}_{44} &= Q_{44}\cos^2(\theta)+Q_{55}\sin^2(\theta)\\ \bar{Q}_{45} &= \tfrac{1}{2}(Q_{55}-Q_{44})\sin(2\theta)\\ \bar{Q}_{55} &= Q_{44}\sin^2(\theta)+Q_{55}\cos^2(\theta)\end{aligned} \tag{4}$$

The Q_{ij} is the plane stress-reduced stiffness given by

$$\begin{aligned}[Q_{11}\quad Q_{12}\quad Q_{22}] &= \left[\tfrac{E_1}{1-\nu_{12}\nu_{21}}\quad \tfrac{\nu_{12}E_2}{1-\nu_{12}\nu_{21}}\quad \tfrac{E_2}{1-\nu_{12}\nu_{21}}\right]\\ [Q_{66}\quad Q_{44}\quad Q_{45}\quad Q_{55}] &= [G_{12}\quad G_{23}\quad G_{12}\quad G_{13}],\end{aligned} \tag{5}$$

where E_1 and E_2 are elastic moduli, ν_{12} and ν_{21} are Poisson's ratios, and G_{12}, G_{13} and G_{23} are the shear moduli. The governing differential equations of motion in form of stresses and moment resultants are

$$\begin{aligned}\delta u_0:\ & \frac{\partial N_{xx}}{\partial x}+\frac{\partial N_{xy}}{\partial y}=I_0\frac{\partial^2 u_0}{\partial t^2}+I_1\frac{\partial^2 \phi_x}{\partial t^2}\\ \delta v_0:\ & \frac{\partial N_{xy}}{\partial x}+\frac{\partial N_{yy}}{\partial y}=I_0\frac{\partial^2 v_0}{\partial t^2}+I_1\frac{\partial^2 \phi_y}{\partial t^2}\\ \delta w_0:\ & \frac{\partial Q_x}{\partial x}+\frac{\partial Q_y}{\partial y}+q+P_{xx}\frac{\partial^2 w_0}{\partial x^2}+2P_{xy}\frac{\partial^2 w_0}{\partial x\partial y}+P_{yy}\frac{\partial^2 w_0}{\partial y^2}=I_0\frac{\partial^2 w_0}{\partial t^2}\\ \delta \phi_x:\ & \frac{\partial M_{xx}}{\partial x}+\frac{\partial M_{xy}}{\partial y}-\phi_x=I_2\frac{\partial^2 \phi_x}{\partial t^2}+I_1\frac{\partial^2 u_0}{\partial t^2}\\ \delta \phi_y:\ & \frac{\partial M_{xy}}{\partial x}+\frac{\partial M_{yy}}{\partial y}-\phi_y=I_2\frac{\partial^2 \phi_y}{\partial t^2}+I_1\frac{\partial^2 v_0}{\partial t^2}\end{aligned} \tag{6}$$

Where the inertia terms are

$$\{I_0,\ I_1,\ I_2\}=\rho\int_{-h/2}^{h/2}\{1,Z,Z^2\}\,dZ \tag{7}$$

The force and moment resultants are given as

$$\begin{Bmatrix} N_{xx} \\ N_{yy} \\ N_{xy} \end{Bmatrix} = \begin{bmatrix} A_{11} & A_{12} & A_{16} \\ A_{12} & A_{22} & A_{26} \\ A_{16} & A_{26} & A_{66} \end{bmatrix} \begin{Bmatrix} \frac{\partial u_0}{\partial x} \\ \frac{\partial v_0}{\partial y} \\ \frac{\partial u_0}{\partial y} + \frac{\partial v_0}{\partial x} \end{Bmatrix} + \begin{bmatrix} B_{11} & B_{12} & B_{16} \\ B_{12} & B_{22} & B_{26} \\ B_{16} & B_{26} & B_{66} \end{bmatrix} \begin{Bmatrix} \frac{\partial \phi_x}{\partial x} \\ \frac{\partial \phi_y}{\partial y} \\ \frac{\partial \phi_x}{\partial y} + \frac{\partial \phi_y}{\partial x} \end{Bmatrix}$$

$$\begin{Bmatrix} M_{xx} \\ M_{yy} \\ M_{xy} \end{Bmatrix} = \begin{bmatrix} B_{11} & B_{12} & B_{16} \\ B_{12} & B_{22} & B_{26} \\ B_{16} & B_{26} & B_{66} \end{bmatrix} \begin{Bmatrix} \frac{\partial u_0}{\partial x} \\ \frac{\partial v_0}{\partial y} \\ \frac{\partial u_0}{\partial y} + \frac{\partial v_0}{\partial x} \end{Bmatrix} + \begin{bmatrix} D_{11} & D_{12} & D_{16} \\ D_{12} & D_{22} & D_{26} \\ D_{16} & D_{26} & D_{66} \end{bmatrix} \begin{Bmatrix} \frac{\partial \phi_x}{\partial x} \\ \frac{\partial \phi_y}{\partial y} \\ \frac{\partial \phi_x}{\partial y} + \frac{\partial \phi_y}{\partial x} \end{Bmatrix} \tag{8}$$

$$\begin{Bmatrix} Q_x \\ Q_y \end{Bmatrix} = \varkappa \begin{bmatrix} A_{44} & A_{45} \\ A_{45} & A_{55} \end{bmatrix} \begin{Bmatrix} \frac{\partial w_0}{\partial y} + \phi_y \\ \frac{\partial w_0}{\partial x} + \phi_x \end{Bmatrix}$$

where $\varkappa$ is the shear correction factor. The laminated in-plane rigidities A_{ij}, B_{ij}, and D_{ij} are defined as

$$\{A_{ij}, B_{ij}, D_{ij}\} = \sum_{k=1}^{N_L} \int_{z_k}^{z_{k+1}} \{1, z, z^2\} dz \,, (i, j = 1, 2, 6) \tag{9}$$

Based on minimum potential energy principle, the governing equations are obtained as follows

$$\int_{t1}^{t2} (\delta U + \delta V - \delta K)\, dt = 0 \tag{6}$$

Meanwhile U, K and V are strain energy, kinematic energy and virtual work done by external forces, respectively. The virtual work done by external forces can be stated as

$$\begin{aligned} \delta V &= -\int_A q(x,y)\, \delta w_0 dA \\ &+ \int_A \left[P_{xx} \frac{\partial w_0}{\partial x} \frac{\delta \partial w_0}{\partial x} + P_{yy} \frac{\partial w_0}{\partial y} \frac{\delta \partial w_0}{\partial y} + P_{xy} \frac{\partial w_0}{\partial x} \frac{\delta \partial w_0}{\partial y} + P_{xy} \frac{\partial w_0}{\partial y} \frac{\delta \partial w_0}{\partial x} \right] dA \end{aligned} \tag{7}$$

where $q(x, y)$ is transverse loading, P_{xx}, P_{yy} and P_{xy} are the constant inplane edge loads. The variation of kinetic energy can be expressed as

$$\begin{aligned} \delta K = -\int_A \{ & I_0(\ddot{u}_0 \delta \dot{u}_0 + \ddot{v}_0 \delta \dot{v}_0 + \ddot{w}_0 \delta \dot{w}_0) + I_1(\ddot{\varphi}_x \delta \dot{u}_0 + \ddot{u}_0 \delta \dot{\varphi}_x + \ddot{\varphi}_y \delta \dot{v}_0 + \ddot{v}_0 \delta \dot{\varphi}_y) + \\ & I_2(\ddot{\varphi}_x \delta \dot{\varphi}_{x0} + \ddot{\varphi}_y \delta \dot{\varphi}_y) \} \, dA \end{aligned} \tag{8}$$

The virtual strain energy is computed as

$$\delta U = \int_V \left[\sigma_{xx} \delta \varepsilon_{xx} + \sigma_{yy} \delta \varepsilon_{yy} + \sigma_{xy} \delta \gamma_{xy} + \sigma_{xz} \delta \gamma_{xz} + \sigma_{yz} \delta \gamma_{xz} \right] dV \tag{10}$$

Substituting Eqs. (7), (8) and (10) into Eq. (6) and integrating by parts, collecting the coefficient's of $\delta u_0, \delta v_0, \delta w_0, \ \delta \varphi_x$ and $\delta \varphi_y$

3. Finite elements formulation

The finite element is a powerful numerical tool that has been used extensively in analysis of composite structures (Fantuzzi and Tornabene 2014a, b). Filippi and Carrera (2016) developed a

finite element formulation with basis of Carrera Unified theory to study the free-vibrational analyses of metallic/composite rotor structures. Errico *et al*. (2019) investigated the effect on the flow-induced vibrations of the lay-up sequence of composite laminated axisymmetric structures, using an hybrid approach based on a wave finite element and a transfer matrix method.

The developed mathematical model defined by Eq. (6) is to be solved to explore the static as well as the dynamic performance of composite plate. The finite elements methodology as an efficient numerical technique is employed for this goal. To derive a computational finite elements model, the virtual work approach (VWA) presents the starting point of a finite element model. According to standard finite element notations, when the total plate domain Ω, shown in Fig. 1 is discretized into *NE* finite elements, one can write the equilibrium between the elastic internal, and inertial forces within each finite element as well as the external applied loads as follows (Assie *et al*. 2011, Abdelrahman *et al*. 2019, Abdelrahman and El-Shafei 2021)

$$\delta K + \delta U - \delta V = 0 \tag{11}$$

where $\delta K, \delta U, \ \delta V$ respectively refer the variation of the total kinetic energy, the variation of the strain energy, and the variation of the work done by the external forces.

The variation of the kinetic energy, δK could be expressed as

$$\delta K = \delta \boldsymbol{q}_e^T \, \boldsymbol{M_e} \, \ddot{\boldsymbol{q}}_{\boldsymbol{e}} = \delta \boldsymbol{q}_e^T \left(\int_{\boldsymbol{A}} \boldsymbol{N^T I \, N} \right) \ddot{\boldsymbol{q}}_{\boldsymbol{e}} dA \tag{12}$$

Variation of the strain energy and work done could be given by

$$\delta U = \delta \boldsymbol{q}_e^T \, \boldsymbol{K_e} \, \boldsymbol{q_e} = \delta \boldsymbol{q}_e^T \left(\int_{\boldsymbol{A}} \boldsymbol{B^T D \, B} dA \right) \boldsymbol{q_e} \tag{13}$$

$$\delta V \ = - \int_A q(x,y) \, \delta w_0 dA \tag{14}$$

where 'e' denotes the elemental division, q_e and $\ddot{q}_e$ refer to vectors of the nodal displacements and accelerations, respectively. M_e and K_e are, respectively, the mass and the stiffness matrices, A is the element area, I is the inertia matrix, B is the strain-displacement, and D is the stress strain relation matrix. The kinematic and the constitutive relations could be expressed as

$$\boldsymbol{\varepsilon} = \boldsymbol{B} \, \boldsymbol{q_e} \ \text{and} \ \boldsymbol{\sigma} = \boldsymbol{D} \, \boldsymbol{\varepsilon} \tag{15}$$

The stress strain relation matrix and the inertia matrix could be expressed as

$$\boldsymbol{\sigma} = \begin{Bmatrix} \sigma_{xx} \\ \sigma_{yy} \\ \tau_{yz} \\ \tau_{xz} \\ \tau_{xy} \end{Bmatrix} = \begin{bmatrix} \bar{Q}_{11} & \bar{Q}_{12} & \mathbf{0} & \mathbf{0} & \bar{Q}_{16} \\ \bar{Q}_{12} & \bar{Q}_{22} & \mathbf{0} & \mathbf{0} & \bar{Q}_{26} \\ \mathbf{0} & \mathbf{0} & \bar{Q}_{44} & \bar{Q}_{45} & \mathbf{0} \\ \mathbf{0} & \mathbf{0} & \bar{Q}_{45} & \bar{Q}_{55} & \mathbf{0} \\ \bar{Q}_{16} & \bar{Q}_{26} & \mathbf{0} & \mathbf{0} & \bar{Q}_{66} \end{bmatrix} \begin{Bmatrix} \varepsilon_{xx} \\ \varepsilon_{yy} \\ \gamma_{yz} \\ \gamma_{xz} \\ \gamma_{xy} \end{Bmatrix}, \qquad \boldsymbol{I} = \begin{bmatrix} \boldsymbol{I_0} & \boldsymbol{I_1} & \mathbf{0} \\ \boldsymbol{I_1} & \boldsymbol{I_2} & \mathbf{0} \\ \mathbf{0} & \mathbf{0} & \boldsymbol{I_0} \end{bmatrix} \tag{16}$$

Assembling the element mass and element stiffness matrices, and the element force vectors transformed into the global coordinate system, the dynamic finite element equations of motion, could be written as

$$\sum_{e=1}^{NE} \boldsymbol{M_e} \ \ddot{\boldsymbol{q}} \ + \sum_{e=1}^{NE} \boldsymbol{K_e} \ \boldsymbol{q} = \boldsymbol{R}, \qquad \boldsymbol{R} \text{ is the overall force vector} \tag{17}$$

with *NE* is the number of elements in the spatial discretized model. The associated boundary conditions for simply supported rectangular plate could be expressed as

$$\begin{aligned} &w_0(x,0) = w_0(x,b) = w_0(0,y) = w_0(a,y) = 0 \\ &\text{and } \psi_x(x,0) = \psi_x(x,b) = \psi_y(0,y) = \psi_y(a,y) \end{aligned} \tag{18}$$

Neglecting the inertial effect leads to the following static problem

$$\sum_{e=1}^{NE} \boldsymbol{K_e}\ \boldsymbol{q} = \boldsymbol{R} \tag{19}$$

Applying the boundary conditions and solve the system of equations in Eq. (19) to obtain the static bending behavior.

On the other hand, neglecting the effect of external load results in the following free vibration problem

$$\sum_{e=1}^{NE} \boldsymbol{M_e}\ \ddot{\boldsymbol{q}} + \sum_{e=1}^{NE} \boldsymbol{K_e}\ \boldsymbol{q} = \boldsymbol{0} \tag{20}$$

To evaluate the natural frequencies and associated normal modes, the solution of the system defined in Eq. (20), which is referred to as the linear eigenvalue problem is required. Assuming that q can be expressed in the following harmonic form

$$\boldsymbol{q} = \boldsymbol{\Lambda e^{iwt}} \text{ and } \ddot{\boldsymbol{q}} = -\boldsymbol{\Lambda w^2 e^{iwt}} = -\boldsymbol{\Lambda \lambda e^{iwt}}, \tag{21}$$

where ω is the natural frequency, λ is the eigen value, $\boldsymbol{\Lambda}$ is the associated eigen vector. Substituting Eg. (21) into Eq. (20) the free vibration analysis is reduced to the following standard eigenvalue extraction problem

$$\sum_{e=1}^{NE} (\boldsymbol{K_e} - \boldsymbol{\lambda M_e})\ \boldsymbol{\Lambda} = \boldsymbol{0} \tag{22}$$

The system of equations defined in (22) has a non-trivial solution only if the dynamic matrix $(\boldsymbol{K_e} - \boldsymbol{\lambda M_e})$ is singular. It can be shown that this condition takes place for a finite number of ω_i^2 or λ_i depending on the order n of the dynamic matrix. The discrete set of values of $\lambda_i, i = 1, 2, 3, \ldots\ldots, n$ 1 are called eigen values. Each eigen value corresponds to an eigen vector, $\boldsymbol{\Lambda_i}$, which is the solution of the following system of equations

$$\sum_{e=1}^{NE} (\boldsymbol{K_e} - \boldsymbol{\lambda_i M_e})\ \boldsymbol{\Lambda_i} = \boldsymbol{0},\ \boldsymbol{i = 1, 2, 3, \ldots\ldots\ldots, n} \tag{23}$$

The eigen value, λ_i and the corresponding eigen vector, $\boldsymbol{\Lambda_i}$ a free vibration mode of the considered composite plate structure.

4. Problem validation

Under this section, a numerical simulation model was developed to validate a published theory on laminated composite sandwich plates using mechanical APDL software. The numerical simulation model was developed based on a published theoretical work by Pagano (1970). The APDL model focuses on the specific case of three-layer symmetric cross-ply ((0°/90°/0°) plates, under sinusoidal load. The validation of the numerical simulation topics is addressed as follows.

Consider a three-layered symmetric cross ply (0°/90°/0°) plate under sinusoidal load. The plate is simply supported on all edges for which had an exact three-dimensional solution by Pagano (1970), as shown in Fig. 1. The plate's layers have equal thicknesses with fibers in the outer layers oriented in the *x*-direction (0°) and those in the inner most layer oriented in the *y*-direction (90°).

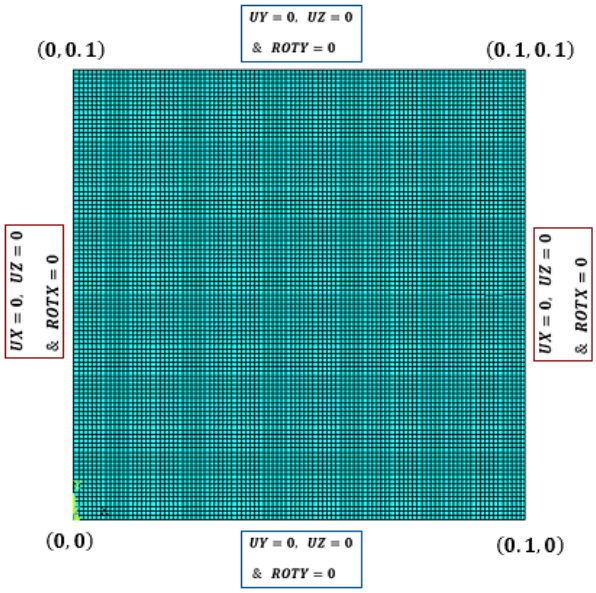

Fig. 1 Simply supported boundary conditions

The material properties provided by Pagano (1970) are listed in Table 1:

Table 1 Pagano's material properties

$E_{11} = 174.6$ GPa	$G_{12} = 3.5$ GPa	$\nu_{12} = 0.25$
$E_{22} = 7$ GPa	$G_{23} = 1.4$ GPa	$\nu_{23} = 0.25$
$E_{33} = 7$ GPa	$G_{13} = 3.5$ GPa	$\nu_{13} = 0.25$

Table 2 Assumption for the APDL validation model

Parameters	Value
Length/Hight Ratio	a/h=100
Length	a=0.100 m
Width	b=0.100 m
Laminate Thick.	h=a/100=0.001 m
Layer Thick.	t=h/3=0.000333 m
Load Type	Sinusoidal
Load Value	q=-10,000 N

where 11 and 22 respectively, are the directions parallel and normal to the fiber's direction. The plate is subjected to a doubly sinusoidal distributed transverse load as in Eq. (1)

$$P_{SDL} = q \sin\left(\frac{\pi x}{a}\right) \sin\left(\frac{\pi y}{b}\right) \tag{24}$$

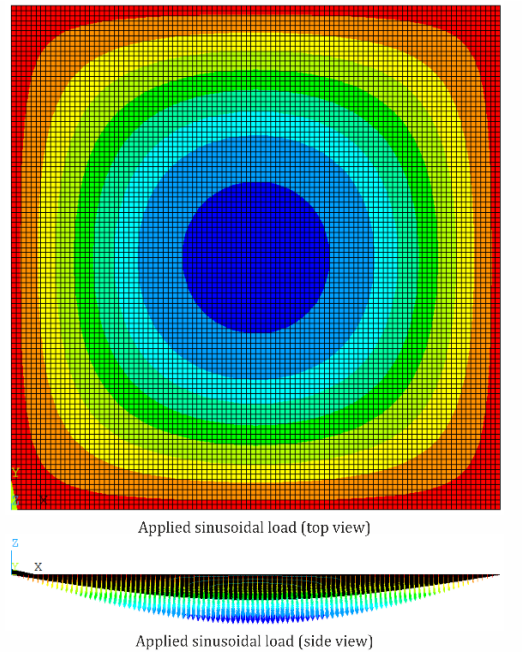

Fig. 2 Static doubly sinusoidal load

Numerical simulation can be a powerful tool in load response analysis and virtual design. Hence, it is required to validate the exact solutions for square (a=b) plate of three-layer symmetric cross-ply (0°/90°/0°) lamination and simply supported on all edges provided by Pagano (1970). The APDL model's assumed input parameters are shown in Table 2 which were used consequently to create the mesh illustrated in Fig. 2 by defining the element type as SHELL181_4 nodes with square element size of 1 mm and applying simply supported boundary conditions. The static doubly sinusoidal load applied to the shell with a magnitude of $q = -10000$ N, is presented in Fig. 3.

The shell and layer results must be adjusted in the APDL General Postproc (Options for Outp). Table 3 represents the deflection and stresses results with APDL output options.

The model's distribution results for; (a) deflection w, (b) normal stress σ_{xx}, (c) normal stress σ_{yy}, (d) shear stress τ_{xy}, (e) shear stress τ_{yz}, and (f) shear stress τ_{xz}, are presented in Fig. 4. However, the obtained results need to be generalized by normalizing the quantities of stresses and deflection by using Eq. (25).

$$\begin{aligned}
\bar{w} &= w\left(\frac{a}{2},\frac{b}{2},0\right)\frac{10^2 E_{22}h^3}{qa^4}\\
\bar{\sigma}_{xx} &= \sigma_{xx}\left(\frac{a}{2},\frac{b}{2},\frac{h}{2}\right)\frac{h^2}{qa^2},\\
\bar{\sigma}_{yy} &= \sigma_{yy}\left(\frac{a}{2},\frac{b}{2},\frac{h}{6}\right)\frac{h^2}{qa^2},\\
\bar{\tau}_{xy} &= \tau_{xy}\left(0,0,\frac{h}{2}\right)\frac{h^2}{qa^2},\\
\bar{\tau}_{xz} &= \tau_{xz}\left(0,\frac{b}{2},0\right)\frac{h}{qa},\\
\bar{\tau}_{yz} &= \tau_{yz}\left(\frac{a}{2},0,0\right)\frac{h}{qa},
\end{aligned} \tag{25}$$

Table 3 Deflection and stresses results with APDL output options

Deflection & Stresses	Shell Results From	FEA Results
w	Top Middle Bottom	0.624 mm
σ_{xx}	Top Bottom	53.9 MPa
σ_{yy}	Top Bottom	18.1 MPa
τ_{xy}	Top Bottom	2.14 MPa
τ_{yz}	Middle	0.103 MPa
τ_{xz}	Top Bottom	0.392 MPa

Table 4 APDL non-dimensionalized deflections and stresses in three-layer (0°/90°/0°) square laminates of *a/h*=100

Deflection & Stresses	Analytical	FEA	Error
$\bar{w}$	Karama *et al*. (2009): 0.4352	0.4368	0.37%
$\bar{\sigma}_{xx}$	Pagano (1970): 0.5390	0.5390	0.00%
$\bar{\sigma}_{yy}$	Pagano (1970): 0.1810	0.1810	0.00%
$\bar{\tau}_{xy}$	Pagano (1970): 0.0213	0.0214	0.47%
$\bar{\tau}_{xz}$	Pagano (1970): 0.3950	0.3939	0.28%
$\bar{\tau}_{yz}$	Pagano (1970): 0.0830	0.1033	24.46%

The model's non-dimensional deflections and stresses in three-layer (0°/90°/0°) square laminates of *a/h*=100 is presented in Table 4. The results of the model analysis are compared with the three-dimensional elasticity results given by Pagano (1970) and compared to the results of the higher shear deformation given by Karama *et al*. (2009). The global average error of each theory is calculated by averaging the absolute values of all the particulars errors presented, and they are presented in the last columns of Table 4. The performance of the model analysis is evaluated by calculating errors compared with both results. The results in Table 4 showed that the finite element model using APDL model provided results that have very good agreement with the results obtained from the analytical models introduced by Pagano (1970), Karama *et al*. (2009). The results of the deflection $\bar{w}$ was not provided by the Pagano (1970) but it was compared to the results given by Karama *et al*. (2009). This good agreement between the analytical and FEA results indicated the model's level reliability and validity. The normal stresses $\bar{\sigma}_{xx}$ and $\bar{\sigma}_{yy}$ results show matching results with the solution of the 3D-elasticity by Pagano (1970). The shear stress $\bar{\tau}_{xy}$ and $\bar{\tau}_{xz}$ results show negligible error when compared to the 3D-elasticity by Pagano (1970). The shear stress $\bar{\tau}_{yz}$ results was higher than the 3D-elasticity by Pagano (1970) by 24.46%. It will be possible to apply the developed APDL model for various fiber orientations, plate geometries, and applied loads if it exhibits a strong connection with the published theories.

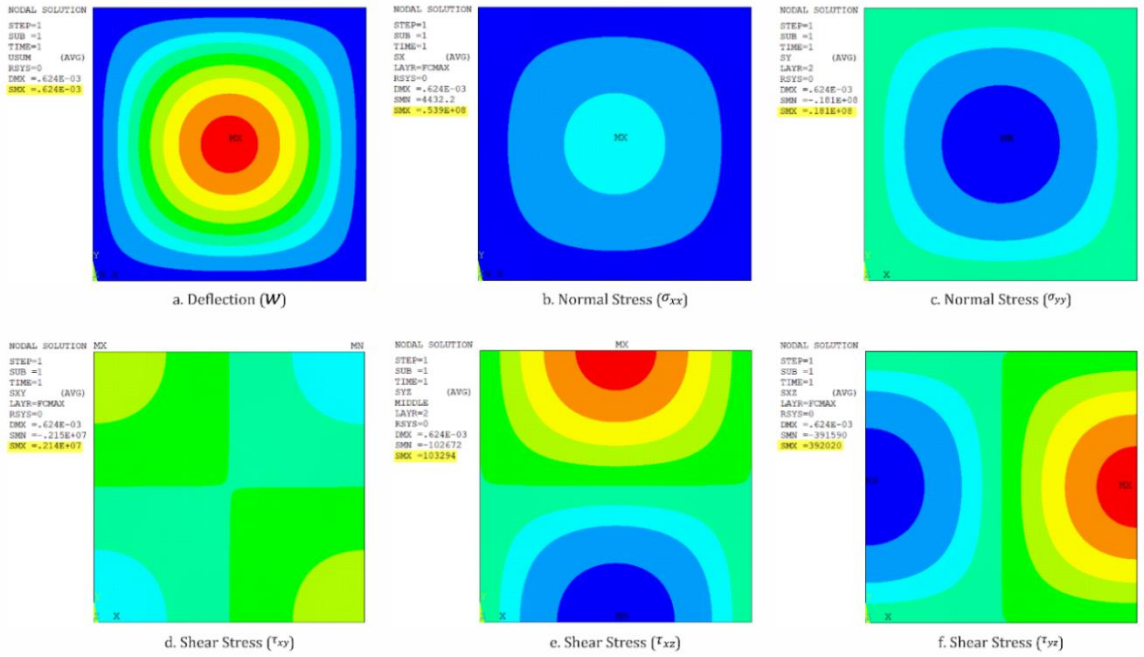

Fig. 3 The distribution results for deflection, normal stresses, and shear stresses from APDL

5. Numerical results

In the second part of this study, different laminated plates with different dimensions and fibers layup orientations including; unidirectional, cross-ply, quasi-Isotropic, and bio-inspired helicoidal have been considered to investigate the load response, in order to improve the performance of the composite structures.

Herein, three different plate dimensions under constant and sinusoidal load were investigated, these plates are presented in Fig. 5 and referred to as case I, II and II and specified as Case I: (a: b) ratio is (1:1), Plate dimensions are 150×150 mm, Case II: (a: b) ratio is (2:1), Plate dimensions are 300×150 mm and Case III: (a: b) ratio is (3:1), Plate dimensions are 450×150 mm. Each lamina consists of 32 unidirectional layers. Each layer thickness is 0.1125 mm, resulting 3.6 mm total lamina thickness. The shell element was defined using the element type SHELL181_4nodes, and square element size of 5 mm. In the three cases, the boundary conditions were fixed supported in the longitudinal ends and simply supported in the lateral sides. Two load conditions were applied to the plate, constant load (P_{CL}) and sinusoidal load (P_{SDL}) as the following Eqs. (8) and (9) where, the load value was $q = -10000$ N for both cases

$$P_{CL} = q,$$
$$P_{SDL} = q \sin\left(\frac{\pi x}{a}\right) \sin\left(\frac{\pi y}{b}\right), \tag{26}$$

The material used in this analysis was prepreg material provided by Cytec with unidirectional 12K HTS carbon fibers which were already pre-impregnated with an 977-2 epoxy matrix. The technical data from the manufacturer and the lamina elastic material properties are listed in Table 5. Heimbs *et al*. (2009).

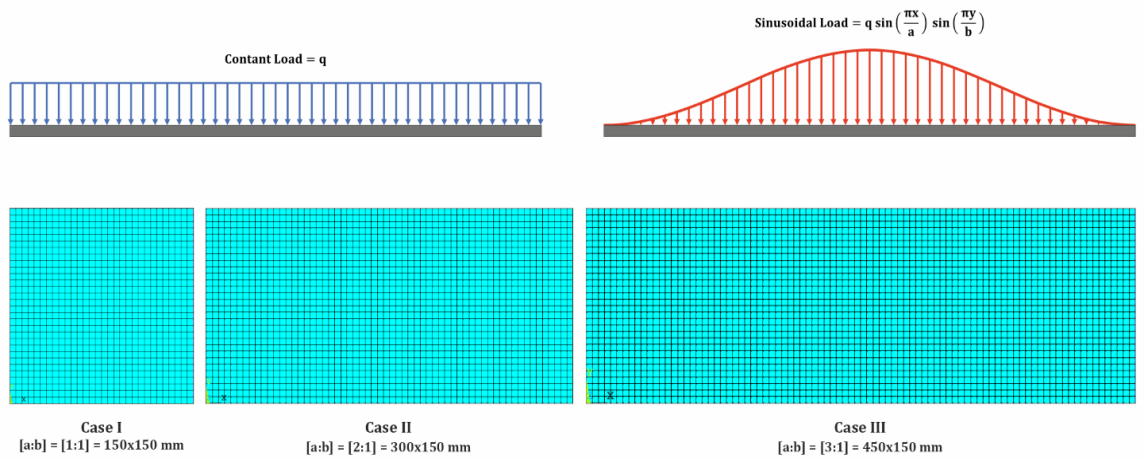

Fig. 4 Different plate geometries and applied loads

Table 5 Material characteristics with mass density of ρ=1620 kg/m^3

$E_{11} = 153$ GPa	$G_{12} = 5.2$ GPa	$\nu_{12} = 0.3$
$E_{22} = 10.7$ GPa	$G_{23} = 2.2$ GPa	$\nu_{23} = 0.3$
$E_{33} = 10.7$ GPa	$G_{13} = 5.2$ GPa	$\nu_{13} = 0.3$

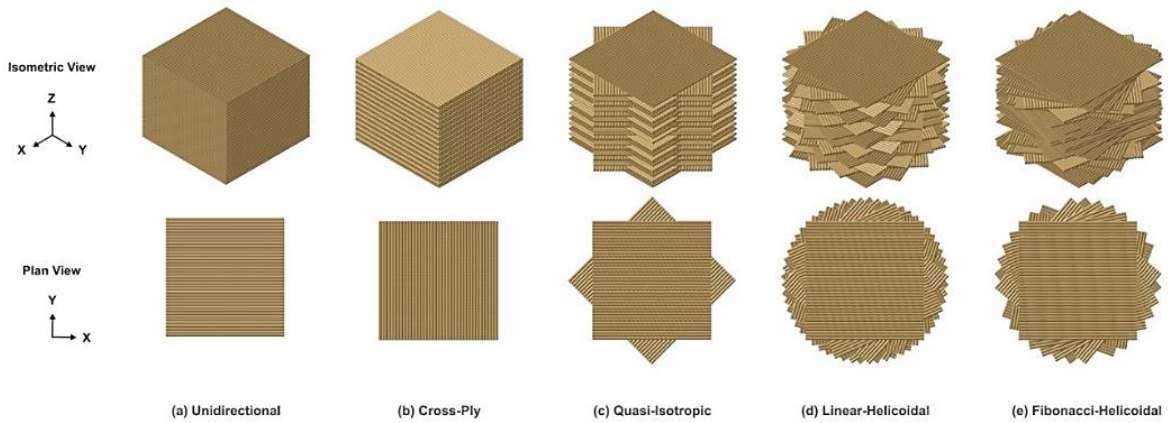

Fig. 5 Different layup configurations examined in this analysis; (a) Unidirectional (UD), (b) Cross-Ply (CP), (c) Quasi-Isotropic (QI), (d) Linear-Helicoidal (LH), and (e) Fibonacci-Helicoidal (FH)

In order to study the effects of fibers orientation on the static load response, different layup configuration was examined including Unidirectional (UD), Cross-Ply (CP), Quasi-Isotropic (QI), the linear bio-inspired known as Linear-Helicoidal 24° (LH) (Wang *et al*. 2021) and non-linear bio-inspired known as Fibonacci-Helicoidal (FH) (Wang *et al*. 2021). The specifications of the different layup configurations are presented in Fig. 6 and Table 6.

The numerical simulation (validation model) used to validate the experimental results was implemeneted for different layup configurations. Only the number of layers was increased from 24 up to 32 layers, which results 3.6 mm total laminate thickness. The analysis results were generated

Table 6 Specifications of the different layup configurations Wang *et al.* (2021)

$Desig.$	N_L	Stacking Sequence
UD	32	Unidirectional $(0^\circ/0^\circ/0^\circ/0^\circ/0^\circ/0^\circ/0^\circ/0^\circ/0^\circ/0^\circ/0^\circ/0^\circ/0^\circ/0^\circ/0^\circ/0^\circ)_s$
CP	32	Cross-Ply - Symmetric $(0^\circ/90^\circ/0^\circ/90^\circ/0^\circ/90^\circ/0^\circ/90^\circ/0^\circ/90^\circ/0^\circ/90^\circ/0^\circ/90^\circ/0^\circ/90^\circ)_s$
QI	32	Quasi-Isotropic - Symmetric $(0^\circ/45^\circ/90^\circ/-45^\circ/0^\circ/45^\circ/90^\circ/-45^\circ/0^\circ/45^\circ/90^\circ/-45^\circ/0^\circ/45^\circ/90^\circ/-45^\circ)_s$
LH	32	Linear-Helicoidal (24°) - Symmetric $(0^\circ/24^\circ/48^\circ/72^\circ/96^\circ/120^\circ/144^\circ/168^\circ/192^\circ/216^\circ/240^\circ/264^\circ/288^\circ/312^\circ/336^\circ/360^\circ)_s$
FH	32	Fibonacci-Helicoidal - ($F_n = F_{n-1} + F_{n-2}, F_0 = 0, F_1 = 10$) - Symmetric $(0^\circ/10^\circ/10^\circ/20^\circ/30^\circ/50^\circ/80^\circ/130^\circ/210^\circ/340^\circ/190^\circ/170^\circ/360^\circ/170^\circ/170^\circ/340^\circ)_s$

Table 7 The maximum non-dimensional deflection and stresses of a CFRP plate under uniform load

$a{:}\,b\ Ratio$	$Desig.$	$\bar{w}$	$\bar{\sigma}_{xx}$	$\bar{\sigma}_{yy}$	$\bar{\tau}_{xy}$	$\bar{\tau}_{yz}$	τ_{xz}
(1: 1)	UD	0.2383	0.2563	0.0276	0.0166	0.0081	0.0466
	CP	0.4072	0.4239	0.0255	0.0193	0.0022	0.0837
	QI	0.3769	0.1642	0.1590	0.1866	0.0146	0.0227
	LH	0.3740	0.3871	0.0218	0.0165	0.0038	0.1048
	FH	0.3028	0.3231	0.0202	0.0146	0.0057	0.0784
(2: 1)	UD	0.1922	0.2203	0.0359	0.0190	0.0316	0.1549
	CP	0.1104	0.1007	0.0228	0.0105	0.0091	0.1570
	QI	0.1080	0.0950	0.1087	0.0865	0.0429	0.0634
	LH	0.1115	0.0988	0.0220	0.0099	0.0120	0.2699
	FH	0.1460	0.1512	0.0289	0.0127	0.0214	0.2274
(3: 1)	UD	0.1075	0.1222	0.0462	0.0154	0.0110	0.0365
	CP	0.0258	0.0302	0.0112	0.0046	0.0020	0.0305
	QI	0.0306	0.0501	0.0618	0.0410	0.0095	0.0141
	LH	0.0312	0.0312	0.0132	0.0048	0.0027	0.0589
	FH	0.0536	0.0485	0.0230	0.0075	0.0055	0.0590

by considering the APDL output options as; shell results from middle shell, and layers results from maximum failure critical.

5.1 Deflection and stresses

The maximum non-dimensional deflection and stresses of the CFRP plate under uniform load and the maximum non-dimensional deflection and stresses of a CFRP plate under sinusoidal load are presented in Table 7 and Table 8; respectively. It is observed that, uniform and sinosoidal loadings, the cross-ply layup configuration *CP* results in largest nondimensional bending deflection, $\bar{\boldsymbol{w}}$ and nondimensional normal stress, $\bar{\boldsymbol{\sigma}}_{\boldsymbol{xx}}$ for aspect ratio, a:b=1 while for for all aspect ratio a:b>1 the maximum nondimensional bending deflection, $\bar{\boldsymbol{w}}$ and the maximum nondimensional normal stress, $\bar{\boldsymbol{\sigma}}_{\boldsymbol{xx}}$ are obtained by unidirectional (*UD*) layup configuration. Regarding the nondimensional shear stress, the largest value of $\bar{\boldsymbol{\tau}}_{\boldsymbol{xy}}$ is produced by QI layup configuration for a:b=1 while for a:b>1, $\boldsymbol{\tau}_{\boldsymbol{xz}}$ shows its largest value for *LH* layup configuration.

Table 8 The maximum non-dimensional bending deflection and stresses of a CFRP plate under sinusoidal load

$a:b$ *Ratio*	*Desig.*	$\bar{w}$	$\bar{\sigma}_{xx}$	$\bar{\sigma}_{yy}$	$\bar{\tau}_{xy}$	$\bar{\tau}_{yz}$	τ_{xz}
	UD	0.1794	0.2016	0.0125	0.0079	0.0014	0.0288
	CP	0.2753	0.3001	0.0193	0.0121	0.0009	0.0453
(1:1)	*QI*	0.2553	0.1227	0.1164	0.1181	0.0068	0.0127
	LH	0.2544	0.2771	0.0172	0.0103	0.0017	0.0586
	FH	0.2117	0.2362	0.0146	0.0086	0.0020	0.0458
	UD	0.1299	0.1570	0.0278	0.0120	0.0131	0.0834
	CP	0.0748	0.0822	0.0161	0.0069	0.0051	0.0615
(2:1)	*QI*	0.0730	0.0694	0.0783	0.0478	0.0248	0.0401
	LH	0.0748	0.0786	0.0157	0.0065	0.0069	0.1710
	FH	0.0979	0.1117	0.0209	0.0084	0.0115	0.1453
	UD	0.0723	0.0902	0.0327	0.0100	0.0058	0.0174
	CP	0.0184	0.0183	0.0084	0.0026	0.0012	0.0080
(3:1)	*QI*	0.0211	0.0374	0.0452	0.0191	0.0058	0.0081
	LH	0.0214	0.0211	0.0095	0.0029	0.0016	0.0340
	FH	0.0363	0.0399	0.0163	0.0049	0.0032	0.0364

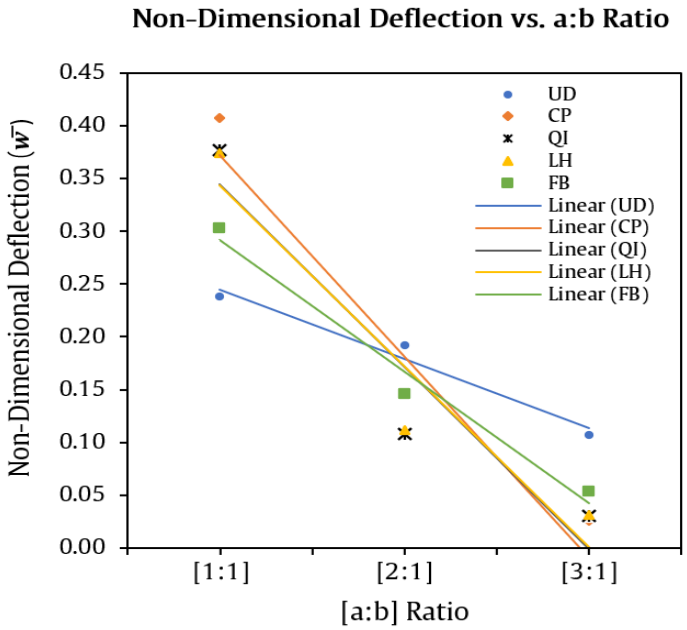

Fig. 6 The maximum nondimesional bending deflection vs. *a*:*b* ratio

Considering the influence of the aspect ratio *a*:*b* on the non-dimensional deflection values, $\bar{\boldsymbol{w}}$ the linear regression of the different layup configurations for different values of the aspect ratio (*a*:*b*) is presented in Fig. 7. It is demonstrated that the maximum nondimensional bending deflection rapidly decreases with increasing the aspect ratio for CP layup configuration. On the other hand, regarding the UD layup configuration, the maximum nondimensional bending deflection slowly decreases with increasing the aspect ratio.

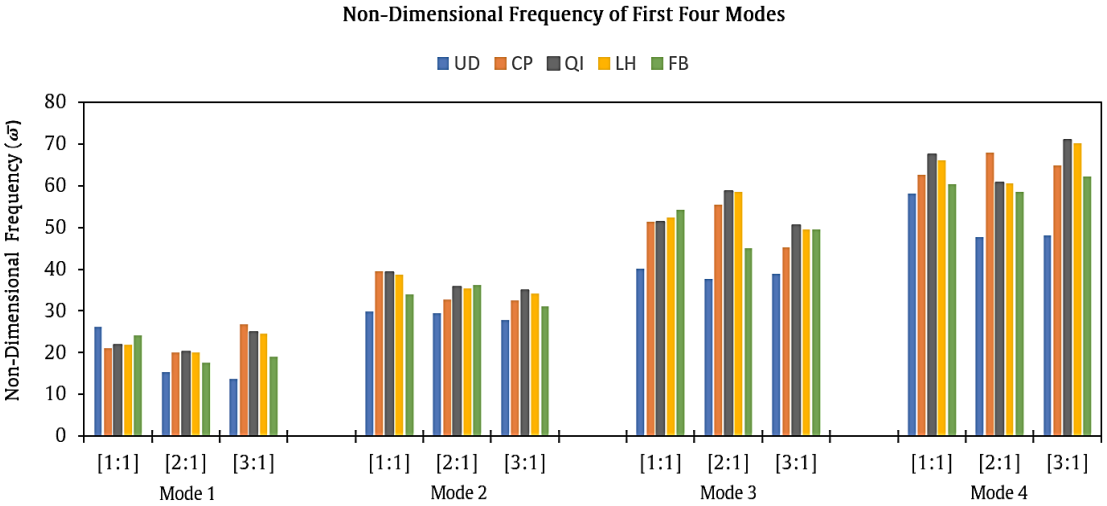

Fig. 7 The first non-dimensional frequency for the first lowest four vibration modes

Table 9 The non-dimensional fundamental frequencies of a CFRP plate

a:b Ratio	*Desig.*	1st Mode $\bar{\omega}_1$	2nd Mode $\bar{\omega}_2$	3rd Mode $\bar{\omega}_3$	4th Mode $\bar{\omega}_4$
	UD	26.2	30.0	40.2	58.1
	CP	21.1	39.4	51.3	62.5
$(1:1)$	QI	21.9	39.4	51.3	67.5
	LH	21.9	38.8	52.3	66.2
	FH	24.1	34.0	54.1	60.4
	UD	15.4	29.5	37.7	47.7
	CP	20.2	32.8	55.3	68.0
$(2:1)$	QI	20.3	35.8	58.7	60.8
	LH	20.0	35.4	58.5	60.5
	FH	17.6	36.2	45.1	58.6
	UD	13.7	27.8	38.9	48.2
	CP	26.7	32.6	45.2	64.8
$(3:1)$	QI	24.9	35.0	50.5	70.9
	LH	24.7	34.2	49.5	70.1
	FH	19.2	31.1	49.6	62.3

5.2 Modal analysis

To generalize the obtained results, the normalized quantities of the fundamental frequencies can be defined using the following equation

$$\bar{\omega} = \omega\left(\frac{a^2}{h}\right)\sqrt{\frac{\rho}{E_2}} \tag{27}$$

The non-dimensional fundamental frequencies of the CFRP plate are presented in Table 9. It may be observed that, the nondimensional frequency parameters decrease with increasing the plate aspect

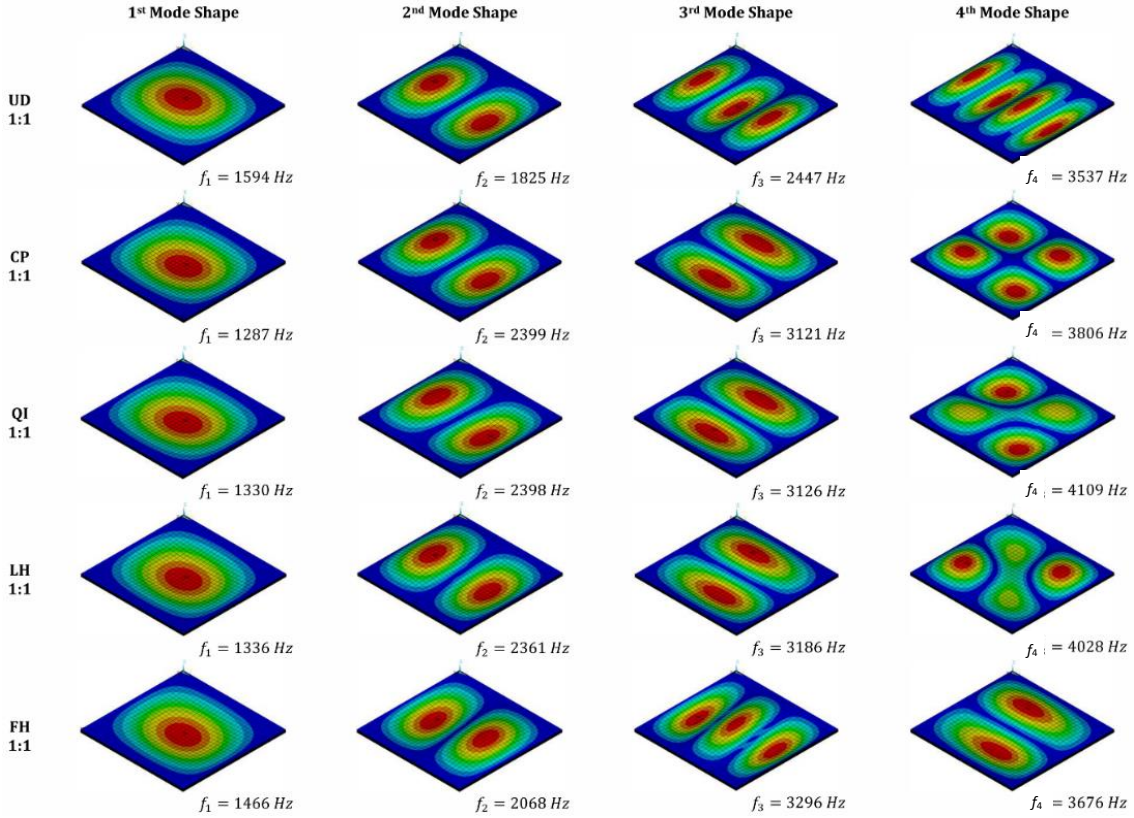

Fig. 8 First four mode shapes of CFRP plate with 1:1 ratio and different layup configuration

ratio for all layup configurations due to the decrease in the overall plate equivalent stiffness to mass ratio. It is also noticed that, for plate aspect ratio 1:1, the largest value of the nondimensional frequency parameters are produced by the UD layup configuration while for the other higher vobration modes, the FH layup configuration produces the largest value of the nondimensional frequency parameters. Increasing the plate aspect ratio, a:b>1, the UD layup plate configuration results in the smallest value of the nondimensional frequency parameter while the FH layup configuration produces the largest values for all vibration modes.

For mor clear illustraton, the comparison between the different plate layup configurations for the first four modes of the non-dimensional fundamental frequency and the a:b ratio is depicted in Fig. 8.

The different mode shapes of the first lowest four vibration modes different plate layup configuration for CFRP plate with different a:b ratio are presented in Figs. 8-10.

6. Conclusions

In the context of finite element simulation, the static, as well as the free vibration behaviors of helicoidal composite plates are quantitatively investigated and analyzed. The dynamic finite elements equations as well as the numerical solution methodology of the helicoidal composite plate

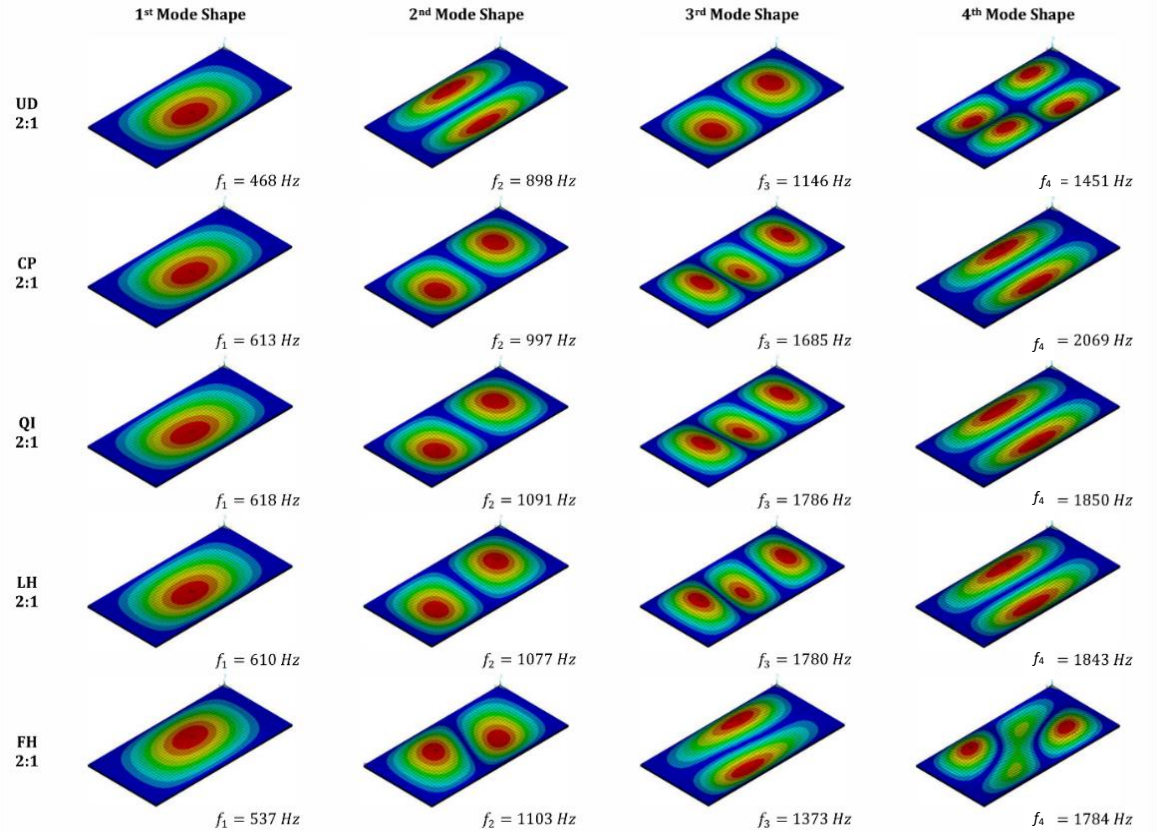

Fig. 9 First four mode shapes of CFRP plate with 2:1 ratio and different layup configuration

are acquired, then mechanical APDL tool is used to obtain and solve the static bending and free vibration problems. Accuracy of the proposed numerical simulation is verified by comparing obtained results the corresponding results reported in the literature. Parametric studies are performed to explore the influences of the lamination scheme the plate aspect ratio on the mechanical performance of the helicoidal composite plate. Notable conclusions based on the numerical results are drawn as follows:

- The overall mechanical performance of helicoidal composite plate significantly affected by the plate layup configuration as well as the plate aspect ratio, a:b. The maximum nondimensional bending deflection, internal stresses, as well as the nondimensional frequency parameters could be controlled by selecting the suitable plate layup configuration for the considered plate aspect ratio.
- In all cases, results obtained from the FEM simulation are in good agreement with the previously outputs reported in the literature.
- The proposed finite element simulation has an acceptable accuracy for utilizing this model for the analysis of more complicated cases.
- Obtained results are supportive for design and manufacturing of such composite structures.

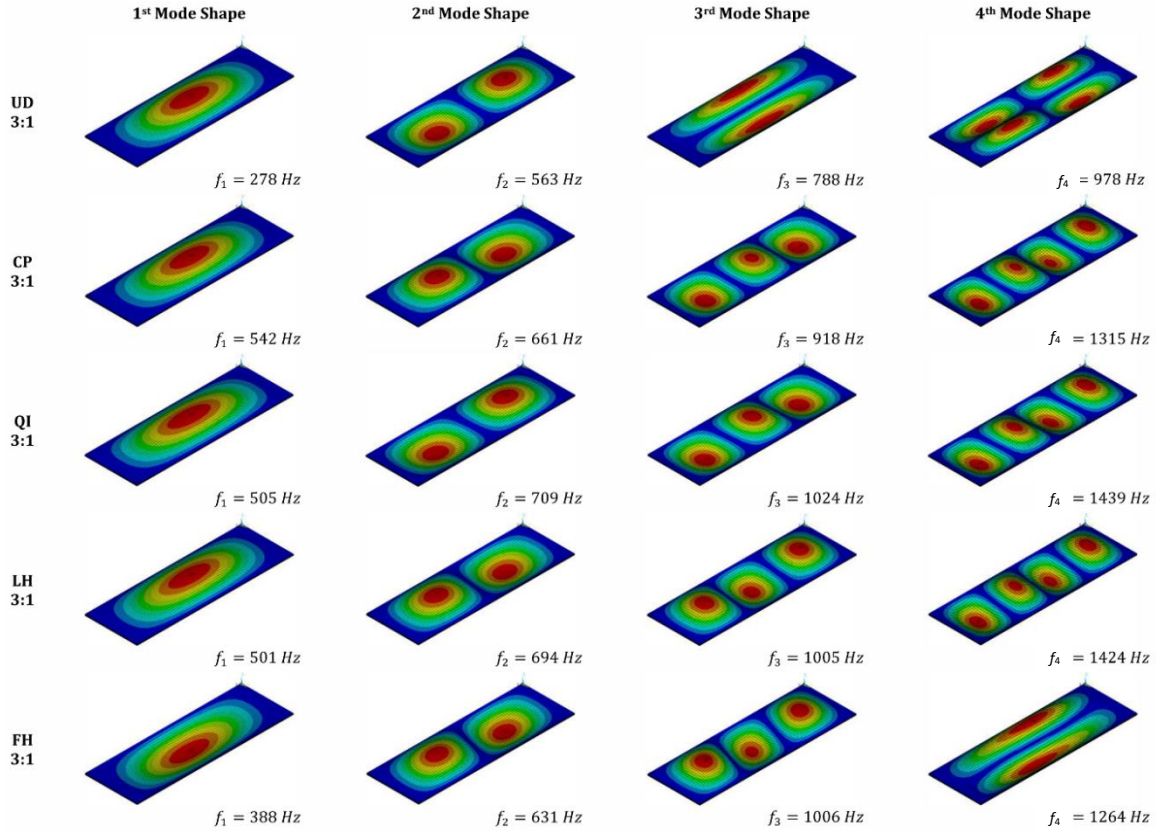

Fig. 10 First four mode shapes of CFRP plate with 3:1 ratio and different layup configuration

Acknowledgement

This research work was funded by the Institutional Fund Project under grant no. (IFPIP: 769-135-1443). The authors gratefully acknowledge technical and financial support provided by the Ministry of Education and King Abdulaziz University, DSR, Jeddah, Saudi Arabia.

References

Abdelrahman, A.A. and El-Shafei, A.G. (2021), "Modeling and analysis of the transient response of viscoelastic solids", *Wave. Random Complex Media*, **31**(6), 1990-2020. https://doi.org/10.1080/17455030.2020.1714790.

Abdelrahman, A.A., El-Shafei, A.G. and Mahmoud, F.F. (2019), "Analysis of steady-state frictional rolling contact problems in Schapery-nonlinear viscoelasticity", *Proc. Inst. Mech. Eng., Part J: J. Eng. Tribol.*, **233**(6), 911-926. https://doi.org/10.1177/1350650118806675.

Abir, M.R., Tay, T.E. and Lee, H.P. (2019), "On the improved ballistic performance of bio-inspired composites", *Compos. Part A: Appl. Sci. Manuf.*, **123**, 59-70. https://doi.org/10.1016/j.compositesa.2019.04.021.

Almitani, K.H., Mohamed, N., Alazwari, M.A., Mohamed, S.A. and Eltaher, M.A. (2022), "Exact solution of

nonlinear behaviors of imperfect bioinspired helicoidal composite beams resting on elastic foundations", *Math.*, **10**(6), 887. https://doi.org/10.3390/math10060887.

Amorim, L., Santos, A., Nunes, J.P. and Viana, J.C. (2021), "Bioinspired approaches for toughening of fibre reinforced polymer composites", *Mater. Des.*, **199**, 109336. https://doi.org/10.1016/j.matdes.2020.109336.

Assie, A.E., Eltaher, M.A. and Mahmoud, F.F. (2011), "Behavior of viscoelastic composite plates under transient load", *J. Mech. Sci. Technol.*, **25**, 1129-1140. https://doi.org/10.1007/s12206-011-0302-6.

Bahmani, A., Li, G., Willett, T.L. and Montesano, J. (2019), "Three-dimensional micromechanical assessment of bio-inspired composites with non-uniformly dispersed inclusions", *Compos. Struct.*, **212**, 484-499. https://doi.org/10.1016/j.compstruct.2019.01.056.

Bar-On, B., Bayerlein, B., Blumtritt, H. and Zlotnikov, I. (2015), "Dynamic response of a single interface in a biocomposite structure", *Phys. Rev. Lett.*, **115**(23), 238001. https://doi.org/10.1103/physrevlett.115.238001.

Bhaskar, D.P. and Thakur, A.G. (2019), "FE modeling for geometrically nonlinear analysis of laminated plates using a new plate theory", *Adv. Aircraft Spacecraft Sci.*, **6**(5), 409-426. https://doi.org/10.12989/aas.2019.6.5.409.

Carrera, E. (2003), "Historical review of zig-zag theories for multilayered plates and shells", *Appl. Mech. Rev.*, **56**(3), 287-308. https://doi.org/10.1115/1.1557614.

Cheng, L., Thomas, A., Glancey, J.L. and Karlsson, A.M. (2011), "Mechanical behavior of bio-inspired laminated composites", *Compos. Part A: Appl. Sci. Manuf.*, **42**(2), 211-220. https://doi.org/10.1016/j.compositesa.2010.11.009.

Errico, F., Franco, F., Ichchou, M., De Rosa, S. and Petrone, G. (2019), "An investigation on the vibrations of laminated shells under aeroacoustic loads using a WFE approach", *Adv. Aircraft Spacecraft Sci.*, **6**, 463-479. https://doi.org/10.12989/aas.2019.6.6.463.

Fantuzzi, N. and Tornabene, F. (2014a), "Strong formulation finite element method for arbitrarily shaped laminated plates-Part I. Theoretical analysis", *Adv. Aircraft Spacecraft Sci.*, **1**(2), 125. https://doi.org/10.12989/aas.2014.1.2.125.

Fantuzzi, N. and Tornabene, F. (2014b), "Strong formulation finite element method for arbitrarily shaped laminated plates-Part II. Numerical analysis", *Adv. Aircraft Spacecraft Sci.*, **1**(2), 145. https://doi.org/10.12989/aas.2014.1.2.145.

Filippi, M. and Carrera, E. (2016), "Capabilities of 1D CUF-based models to analyse metallic/composite rotors", *Adv. Aircraft Spacecraft Sci.*, **3**(1), 1. https://doi.org/10.12989/aas.2016.3.1.001.

Garg, A., Belarbi, M.O., Chalak, H.D., Li, L., Sharma, A., Avcar, M., ... & Gulia, R. (2023), "Buckling and free vibration analysis of bio-inspired laminated sandwich plates with helicoidal/Bouligand face sheets containing softcore", *Ocean Eng.*, **270**, 113684. https://doi.org/10.1016/j.oceaneng.2023.113684.

Haldar, S. and Bruck, H. A. (2014), "Mechanics of composite sandwich structures with bioinspired core", *Compos. Sci. Technol.*, **95**, 67-74. https://doi.org/10.1016/j.compscitech.2014.02.011.

Han, Q., Chen, S., Wang, J., Han, J., Shi, S., Li, R., ... & Ren, L. (2023), "Biomimetic laminated basalt fiber-reinforced composite with sinusoidally architected helicoidal structure integrating superior mechanical properties and microwave-transmissibility", *Compos. Sci. Technol.*, **231**, 109836. https://doi.org/10.1016/j.compscitech.2022.109836.

Han, Q., Li, H., Chen, X., Shi, S., Shao, R., Li, B. and Han, Z. (2022), "Impact resistant basalt fiber-reinforced aluminum laminate with Janus helical structures inspired by lobster and mantis shrimp", *Compos. Struct.*, **291**, 115551. https://doi.org/10.1016/j.compstruct.2022.115551.

Han, Q., Qin, H., Liu, Z., Han, Z., Zhang, J., Niu, S., ... & Shi, S. (2020), "Experimental investigation on impact and bending properties of a novel dactyl-inspired sandwich honeycomb with carbon fiber", *Constr. Build. Mater.*, **253**, 119161. https://doi.org/10.1016/j.conbuildmat.2020.119161.

Heimbs, S., Heller, S., Middendorf, P., Hähnel, F. and Weiße, J. (2009), "Low velocity impact on CFRP plates with compressive preload: Test and modelling", *Int. J. Impact Eng.*, **36**(10-11), 1182-1193. https://doi.org/10.1016/j.ijimpeng.2009.04.006.

Jayatilake, I. N., Karunasena, W. and Lokuge, W. (2016), "Finite element based dynamic analysis of multilayer fibre composite sandwich plates with interlayer delaminations", *Adv. Aircraft Spacecraft Sci.*, **3**(1), 15.

https://doi.org/10.12989/aas.2016.3.1.015.
Kaci, D.A., Madani, K., Mokhtari, M., Feaugas, X. and Touzain, S. (2017), "Impact of composite patch on the J-integral in adhesive layer for repaired aluminum plate", *Adv. Aircraft Spacecraft Sci.*, **4**(6), 679. https://doi.org/10.12989/aas.2017.4.6.679.
Karama, M., Afaq, K.S. and Mistou, S. (2009), "A new theory for laminated composite plates", *Proc. Inst. Mech. Eng., Part L: J. Mater.: Des. Appl.*, **223**(2), 53-62. https://doi.org/10.1243/14644207jmda189.
Karamanli, A., Eltaher, M.A., Thai, S. and Vo, T.P. (2023), "Transient dynamics of 2D-FG porous microplates under moving loads using higher order finite element model", *Eng. Struct.*, **278**, 115566. https://doi.org/10.1016/j.engstruct.2022.115566.
Lee, S., Lim, D.D., Pegg, E. and Gu, G.X. (2022), "The origin of high-velocity impact response and damage mechanisms for bioinspired composites", *Cell Report. Phys. Sci.*, **3**(12), 1. https://doi.org/10.1016/j.xcrp.2022.101152.
Liew, K.M., Zhao, X. and Ferreira, A.J. (2011), "A review of meshless methods for laminated and functionally graded plates and shells", *Compos. Struct.*, **93**(8), 2031-2041. https://doi.org/10.1016/j.compstruct.2011.02.018.
Magrini, T., Senol, A., Style, R., Bouville, F. and Studart, A.R. (2022), "Fracture of hierarchical multi-layered bioinspired composites", *J. Mech. Phys. Solid.*, **159**, 104750. https://doi.org/10.1016/j.jmps.2021.104750.
Mantari, J.L., Oktem, A.S. and Soares, C.G. (2011), "Static and dynamic analysis of laminated composite and sandwich plates and shells by using a new higher-order shear deformation theory", *Compos. Struct.*, **94**(1), 37-49. https://doi.org/10.1016/j.compstruct.2011.07.020.
Melaibari, A., Wagih, A., Basha, M., Kabeel, A.M., Lubineau, G. and Eltaher, M.A. (2021), "Bio-inspired composite laminate design with improved out-of-plane strength and ductility", *Compos. Part A: Appl. Sci. Manuf.*, **144**, 106362. https://doi.org/10.1016/j.compositesa.2021.106362.
Mohamed, S.A., Mohamed, N. and Eltaher, M.A. (2022a), "Bending, buckling and linear vibration of bio-inspired composite plates", *Ocean Eng.*, **259**, 111851. https://doi.org/10.1016/j.oceaneng.2022.111851.
Mohamed, S.A., Mohamed, N. and Eltaher, M.A. (2022b), "Snap-through instability of helicoidal composite imperfect beams surrounded by nonlinear elastic foundation", *Ocean Eng.*, **263**, 112171. https://doi.org/10.1016/j.oceaneng.2022.112171.
Moosazadeh, H. and Mohammadi, M.M. (2021), "Two-dimensional curved panel vibration and flutter analysis in the frequency and time domain under thermal and in-plane load", *Adv. Aircraft Spacecraft Sci.*, **8**(4), 345-372. https://doi.org/10.12989/aas.2021.8.4.345.
Pagano, N.J. (1970), "Exact solutions for rectangular bidirectional composites and sandwich plates", *J. Compos. Mater.*, **4**(1), 20-34. https://doi.org/10.1177/002199837000400102.
Rachid, Z., Kaddour, R. and Achache, H. (2018), "Dynamic calculation of a tapered shaft rotor made of composite material", *Adv. Aircraft Spacecraft Sci.*, **5**(1), 51. https://doi.org/10.12989/aas.2018.5.1.051.
Reddy, J.N. (1990), "A review of refined theories of laminated composite plates", *Shock Vib. Digest*, **22**(7), 3-17. https://doi.org/10.1177/058310249002200703.
Reddy, J.N. (2003). *Mechanics of Laminated Composite Plates and Shells: Theory and Analysis*, CRC Press.
Sojobi, A.O. and Liew, K.M. (2022), "Multi-objective optimization of high performance bio-inspired prefabricated composites for sustainable and resilient construction", *Compos. Struct.*, **279**, 114732. https://doi.org/10.1016/j.compstruct.2021.114732.
Wang, H., Wang, C., Hazell, P.J., Wright, A., Zhang, Z., Lan, X., ... & Zhou, M. (2021), "Insights into the high-velocity impact behaviour of bio-inspired composite laminates with helicoidal lay-ups", *Polym. Test.*, **103**, 107348. https://doi.org/10.1016/j.polymertesting.2021.107348.
Yang, F. and Xie, W. (2022), "Thermal buckling behavior of Bouligand inspired laminated composite plates", *J. Compos. Mater.*, **56**(26), 3939-3947. https://doi.org/10.1177/00219983221125905.
Yang, F., Xie, W. and Meng, S. (2020), "Global sensitivity analysis of low-velocity impact response of bio-inspired helicoidal laminates", *Int. J. Mech. Sci.*, **187**, 106110. https://doi.org/10.1016/j.ijmecsci.2020.106110.
Zhang, B., Yang, J., Li, Y., Zhang, J., Niu, S., Han, Z. and Ren, L. (2023), "Bioinspired basalt fiber composites with higher impact resistance through coupling sinusoidal and helical structures inspired by mantis shrimp",

Int. J. Mech. Sci., **244**, 108073. https://doi.org/10.1016/j.ijmecsci.2022.108073.
Zhang, Y.X. and Yang, C.H. (2009), "Recent developments in finite element analysis for laminated composite plates", *Compos. Struct.*, **88**(1), 147-157. https://doi.org/10.1016/j.compstruct.2008.02.014.

CC